ARTICLE OPEN

Check for updates

A novel role of the antidepressant paroxetine in inhibiting neuronal Kv7/M channels to enhance neuronal excitability

Huan Shi[1,3], Qinqin Li[1,3], Fang Hu[1,2], Yani Liu[1,2]✉ and KeWei Wang[1,2]✉

The voltage-gated Kv7/KCNQ/M potassium channels exert inhibitory control over neuronal membrane excitability. The reduction of Kv7 channel function can improve neuronal excitability that defines the fundamental mechanism of learning and memory. This suggests that pharmacological inhibition of Kv7 channels may present a therapeutic strategy for cognitive improvement. Paroxetine, a selective serotonin reuptake inhibitor, is widely used in the treatment of various types of depression with reported improvements in memory and attention. However, the exact mechanism underlying cognitive improvement by paroxetine remains poorly understood. In this study, we demonstrate that paroxetine inhibits whole-cell Kv7.2/Kv7.3 channel currents in a concentration-dependent manner with an IC_{50} of 3.6 ± 0.2 μM. In single-channel recording assay, paroxetine significantly reduces the open probability of Kv7.2/Kv7.3 channels. Moreover, paroxetine exhibits an inhibition of the native M-current and an increase in the firing of action potentials in hippocampal neurons. Taken together, our findings unveil a novel role of the antidepressant paroxetine in inhibiting M-current, providing insights into its pharmacological effects on cognition enhancement.

Translational Psychiatry (2025)15:116 ; https://doi.org/10.1038/s41398-025-03291-w

INTRODUCTION

The voltage-gated Kv7 potassium channel family consists of five members, Kv7.1–Kv7.5, also known as KCNQ1-KCNQ5, which are encoded by *KCNQ1-KCNQ5* genes [1, 2]. While Kv7.1 is mainly expressed in cardiac tissue [3, 4] and Kv7.4 is predominantly found in the hair cells of the inner ear [5, 6], the other three subunits (Kv7.2, Kv7.3 and Kv7.5) are primarily expressed in the nervous system where they form the molecular basis of the native M-current [2, 7, 8].

The M-current, first identified by Brown and colleagues in the sympathetic ganglion of the bullfrog [9], is a slowly activating and deactivating K^+ current. It is named for its inhibition upon activation of G protein-coupled muscarinic acetylcholine receptors (mAChRs) [10]. The M-current is mainly generated from heteromeric combinations of Kv7.2 and Kv7.3 channels [7]. With an activation threshold close to the resting membrane potential of neurons, the opening of M-channel induces a sustained outward K^+ current, thereby reducing neuronal excitability [2, 11, 12]. Consequently, it presents a potential pharmacological target for diseases associated with hyperexcitability, such as epilepsy and pain [13, 14]. Conversely, inhibition of M-current can increase neuronal firings [15, 16], enhance neurotransmitters release [17], and facilitate the induction of long-term potentiation (LTP) in hippocampal neurons [18–21]. In addition, Kv7 inhibitors, including linopirdine and XE991, have been reported to enhance learning and memory abilities in rodents [22–24]. These observations underscore the crucial role of M-current inhibition in learning and memory, suggesting as potential as a therapeutic strategy for cognitive deficits.

Cognitive dysfunction is a highly relevant dimension of psychiatric disorders including major depressive disorder (MDD), Alzheimer's disease (AD) and Parkinson's disease (PD) [25]. Patients with MDD exhibit various cognitive impairments, such as working memory and attention [26–28]. Antidepressant paroxetine, a selective serotonin reuptake inhibitor (SSRI), is widely used to treat depression, post-traumatic stress disorder, generalized anxiety disorder and other psychiatric disorders [29, 30]. First marketed in 1992, paroxetine remains a common clinical choice for these psychiatric disorders and is also prescribed off-label drug for indications, such as premature ejaculation in men, and vasomotor symptoms (e.g. hot flashes and night sweats) in menopausal women [31–35]. Clinical and experimental evidences demonstrate that paroxetine can alleviate memory loss and attentional deficits in patients with depression [36], as well as improve memory deficits in APP/PS1 [37] and 3xTg AD model mice [38]. In addition, paroxetine has been reported to inhibit several ion channels related to neuronal excitability, including G protein-activated inwardly rectifying K^+ channels (GIRK) [39] and Kv3.1 channel [40]. These observations led us to hypothesize that paroxetine might also inhibit Kv7/M channels.

To test this hypothesis, we investigated the pharmacological effects of paroxetine on Kv7/M channels. Our findings demonstrate that paroxetine concentration-dependently inhibits macroscopic and single-channel currents of Kv7.2/Kv7.3 channels expressed in HEK293T cells. Furthermore, paroxetine suppresses the native M-current in hippocampal neurons and increases neuronal firings. These results suggest that the

[1]Department of Pharmacology, School of Pharmacy, Qingdao University Medical college, Qingdao, China. [2]Institute of Innovative Drugs, Qingdao University, Qingdao, China. [3]These authors contributed equally: Huan Shi, Qinqin Li. ✉email: liuyani@qdu.edu.cn; wangkw@qdu.edu.cn

Received: 20 June 2024 Revised: 18 January 2025 Accepted: 18 February 2025
Published online: 02 April 2025

cognitive improvements associated with paroxetine are directly linked to its inhibition of neuronal Kv7/M channels.

METHODS AND MATERIALS

Drugs and chemicals

Antidepressant paroxetine hydrochloride was purchased from TargetMol (Boston, MA, USA). Tool compounds, including retigabine (RTG), were purchased from MedChemExpress (New Jersey, USA) and XE991 was from Abcam (Cambridge, UK). Stock solutions of paroxetine (200 mM), RTG (100 mM) and XE991 (100 mM) were dissolved in dimethyl sulfoxide (DMSO) and stored at −20 °C.

Cell culture and transfection

The cDNAs for hKv7.1 (NM000218), hKv7.2 (AF110020), hKv7.4 (AF105202) and hKv7.5 (AF249278) were cloned into vector pcDNA3.1. Chinese hamster ovary (CHO) cells stably expressing Kv7.2/Kv7.3 channels (constructed in-house without mycoplasma infection) were cultured in F12 medium (Thermo Fisher, Waltham, MA, USA) containing 10% fetal bovine serum (FBS, PAIN, Australia), 600 μg/mL G418 (MedChemExpress, New Jersey, USA) and Chloramphenicol B (Sigma, MO, USA). Human embryonic kidney 293 T (HEK293T) cells (without mycoplasma infection) were maintained in DMEM (Thermo Fisher, Waltham, MA, USA) supplemented with 10% FBS. All cells were incubated in a constant temperature incubator at 37 °C with 5% CO_2. The cDNA plasmid expressing the target gene together with green fluorescent protein (GFP) was co-transfected into HEK293T cells using lipofectamine 2000 (Thermo Fisher, Waltham, MA, USA) following the manufacturer's instructions. Electrophysiological recordings were performed 24 h after transfection.

Isolation and culture of rat hippocampal neurons

Primary hippocampal neurons were isolated and cultured as previously described [41, 42]. Briefly, hippocampus was rapidly isolated from 24-h newborn SD rat (Beijing Vital River Laboratory Animal Technology Co., Ltd, China) brains, stripped as cleanly as possible, centrifuged after digestion with 0.05% trypsin (Thermo Fisher, Waltham, MA, USA) before resuspended and seeded with approximately 2×10^4 cells on each coverslip pre-coated with poly-D lysine (Thermo Fisher, Waltham, MA, USA). Patch-clamp recordings were performed after 14–16 days of culture with Neurobasal Medium (Thermo Fisher, Waltham, MA, USA) supplemented with 2% B-27 (Thermo Fisher, Waltham, MA, USA) and 0.5 mM GlutaMax (Thermo Fisher, Waltham, MA, USA). All in vivo animal procedures were approved by the Committee of Animal Care and Use Center of Qingdao University (Qingdao, China).

Electrophysiology

Whole-cell recordings. The CHO cells stably expressing Kv7.2/Kv7.3 channels and HEK293T cells transiently transfected with Kv7 cDNAs were recorded using a perforated patch-clamp technique with amphotericin B (250 μg/mL, Sigma, MO, USA) in the pipette solution. The tips of patch electrodes (2–5 MΩ) were dipped into the intracellular solution for 1–5 s for backfill with the intracellular solution supplemented with amphotericin B. Data were acquired at 10 kHz and filtered at 2 kHz using a HEKA EPC10 amplifier (Harvard Bioscience, Holliston, MA, USA). The intracellular solution consisted of (in mM): KCl 150, $MgCl_2$ 5, and HEPES 10; pH 7.4 adjusted with KOH. The extracellular solution was prepared as follows (in mM): NaCl 160, KCl 2.5, $MgCl_2$ 1, $CaCl_2$ 2, glucose 10, and HEPES 20 at pH 7.4 adjusted with NaOH.

Single-channel recordings. Single-channel recordings in cell-attached configuration were performed as previously described [43]. Data were acquired at 1 kHz and filtered at 0.8–1 kHz using a Multiclamp 700B (Molecular Devices, CA, USA). Pipettes had resistances of 8–10 MΩ when filled with the bath solution consisting of the following composition (in mM): 150 NaCl, 5 KCl, 1 $MgCl_2$, 2 $CaCl_2$ and 10 HEPES, pH 7.4 with NaOH. The resting membrane potentials (RMP) of HEK293T cells transfected with Kv7.2/Kv7.3 and Kv7.2 channels were −46.6 ± 2.0 mV and −37.7 ± 1.0 mV tested using current-clamp recording approach when the pipette was filled with intracellular solution including (mM): K-gluconate 150, EGTA 2, $CaCl_2$ 1, $MgCl_2$ 1, HEPES 10 (pH 7.3 adjusted with KOH). The Kv7.2/Kv7.3 and Kv7.2 single channel currents were elicited by a depolarizing potential at 0 mV, which is calculated with a function: V_m=RMP-$V_{pipette}$.

M-current and action potential recordings. Hippocampal neurons cultured for 14–16 d were used to record M-current and action potentials using a whole-cell patch clamp technique. The composition of the intracellular solution was as follows (in mM): K-gluconate 100, KCl 50, EGTA10, $MgCl_2$ 5, and HEPES 2 at pH 7.3 adjusted with KOH. The extracellular solution contained (in mM): NaCl 140, KCl 3, $CaCl_2$ 2, $MgCl_2$ 2, HEPES 10, and glucose 10, pH7.4 with NaOH. To record native M-current in hippocampal neurons, tetrodotoxin (1 μM) supplemented in the extracellular solution was used to block sodium channels. For recordings of action potentials and membrane potentials, the extracellular solution was supplemented with ionotropic glutamate NMDA and non-NMDA receptor inhibitors DL-2-amino-5-phosphonovaleric acid and 6,7-dinitroquinoxaline-2,3-dione (each at 20 μM); and GABA receptors bicuculline and baclofen (each at 10 μM). All experiments were conducted at room temperature.

Molecular docking and site mutations

Molecular docking was performed using the MOE 2020. Human Kv7.2 cryo-electron microscopy structure (PDB: 7CR0) was obtained from the Protein Data Bank. The 3D structure of paroxetine was obtained from the PubChem database and processed using Energy Minimized of MOE. Protein structure was processed using QuickPrep of MOE prior to docking for correction of structural problems, protonation, removal of unbound water molecules, and energy optimization. The pocket was selected using the MOE 2020 Unique Functional Site Finder (based on PLB scores). Default parameters were chosen for docking and the lowest binding energy was used to visualize ligand–protein interactions. Mutations of the channel amino acid residues to alanine were performed following the instruction of Mut Express® II Fast Mutagenesis Kit V2 (Vazyme, Nanjing, China) and verified by sequencing (Qingke, Beijing, China).

Statistics

Data were analyzed using software including Clampfit 10.7, Patchmaster, OriginPro 8.0, GraphPad Prism 6.0, Adobe Illustrator 10, and Igor Pro (Wavemetrics). The concentration-response curve was fitted using the logistic function of $y=A_2+[(A_1-A_2)/(1+(x/x_0)^P]$. The activation curves were fitted with a Boltzmann function of $y=\max/[1+\exp(V_{1/2}-V)/k]$. The activation and deactivation time constants were fitted to a single exponential function of $I=A\times[1-\exp(-t/\tau)]$. All data were expressed as the mean ± SEM. Statistical significance between experimental groups was evaluated using a paired Student's *t*-test and one-way ANOVA with a significance level set at $P < 0.05$.

RESULTS

Concentration-dependent inhibition of macroscopic Kv7.2/Kv7.3 currents and single-channels by paroxetine

We began by testing the effect of paroxetine on Kv7.2/Kv7.3 currents stably expressed in CHO cells using a perforated whole-cell patch-clamp recording assay. Paroxetine at 3 μM inhibited Kv7.2/Kv7.3 currents recorded at 0 mV by 62.8 ± 6.5% (Fig. 1A, $n = 5$). As a positive control, M-current inhibitor XE991 at 3 μM inhibited Kv7.2/Kv7.3 currents by 81.4 ± 1.5% (Fig. 1A, $n = 5$). Perfusion with different concentrations of paroxetine, ranging from 1–100 μM, resulted in a concentration-dependent inhibition of Kv7.2/Kv7.3 currents with an IC_{50} of 3.6 ± 0.2 μM (Fig. 1B and Table 1, $n = 5$). We further examined the effect of paroxetine on voltage-dependent activation of Kv7.2/Kv7.3 channels. At a concentration near its IC_{50} of 3 μM, paroxetine exhibited no significant effect on voltage-gated activation of Kv7.2/Kv7.3 currents with the $V_{1/2}$ value from −3.9 ± 1.2 mV to −7.5 ± 3.5 mV (Fig. 1C and Table 1, $n = 8$). In addition, paroxetine slowed the activation kinetic of Kv7.2/Kv7.3 channels with an increased time constant to 112.8 ± 9.0 ms from 94.5 ± 11.0 ms, while there was no significant alteration in deactivation kinetic (from 14.4 ± 1.1 ms to 12.6 ± 0.7 ms) (Fig. 1D and Table 2, $n = 5$).

We further tested the effect of paroxetine on Kv7.2/Kv7.3 single-channels using single-channel recordings in the cell-attached configuration. Paroxetine at 3 μM significantly decreased the open probability of Kv7.2/Kv7.3 single-channels to 0.13 ± 0.01, compared to 0.28 ± 0.01 in the control, without altering the single-channel conductance, which remained at 10.4 ± 0.9 pS as compared to 10.9 ± 1.1 pS in the control (Fig. 2, $n = 5$).

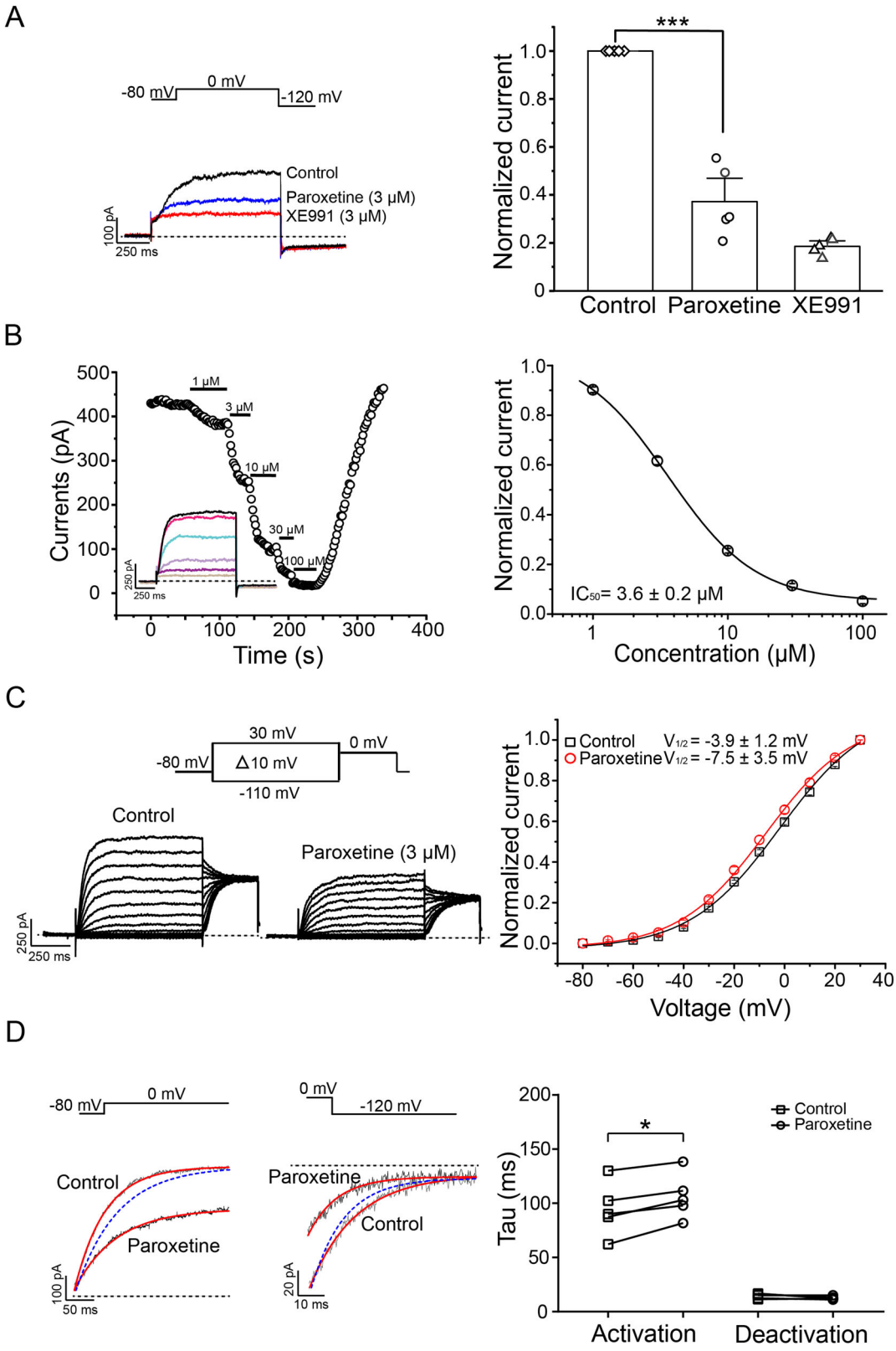

Concentration-dependent inhibition of Kv7.2 current by paroxetine

Kv7.2 channel is an essential component of native M-current in neurons and can form a functional homotetramer independent of Kv7.3. We next tested the effect of paroxetine on Kv7.2 channel expressed in HEK293T cells. Paroxetine concentration-dependently inhibited Kv7.2 current with an IC_{50} of 12.3 ± 6.5 μM (Fig. 3A and Table 1, $n = 9$). We also examined the effect of paroxetine on the voltage-dependent activation of Kv7.2 at a concentration near its IC_{50}. As shown in Fig. 3B, paroxetine at

Fig. 1 Concentration-dependent inhibition of Kv7.2/Kv7.3 currents by paroxetine. A Left panel, representative Kv7.2/Kv7.3 current traces elicited by depolarizing potential at 0 mV before and after application of paroxetine (3 μM) or positive control XE991 (3 μM). The dotted line represents zero current level; Right panel, summary for normalized current from left panel ($n = 5$), paired *t*-test, $^{***}P < 0.001$. **B** Left panel, concentration-dependent inhibition of Kv7.2/Kv7.3 currents by paroxetine. Representative current traces from each concentration of paroxetine are shown in the inset; Right panel, data from the left panel were fitted with Logistic function and IC_{50} of 3.6 ± 0.2 μM was obtained ($n = 5$). **C** Left panels, representative current traces from Kv7.2/Kv7.3 channels in response to depolarizing voltage steps from −110–30 mV with an increment of 10 mV followed by a pulse at 0 mV in the absence (left panel) and presence (middle panel) of paroxetine; Right panel, activation curves of Kv7.2/Kv7.3 currents in the absence or presence of paroxetine measured at the beginning of the 0 mV and fitted with Boltzmann function ($n = 8$). **D** Superimposed activation traces generated at 0 mV (left panel) and deactivation traces at −120 mV (middle panel) before and after paroxetine (3 μM). The current traces from paroxetine were scaled up to the same current amplitude of the control (blue dotted line); Right panel, summary of the effect of paroxetine on activation and deactivation time constants of Kv7.2/Kv7.3 fitted with a single exponential function ($n = 5$), paired *t*-test, $^{*}P < 0.05$. All data were expressed as the mean±SEM.

Table 1. Concentration-dependent inhibition and rightward shift of Kv7 subtype activation curves by paroxetine.

Subfamily member	IC_{50} (μM)	Control $V_{1/2}$ (mV)	Paroxetine $V_{1/2}$ (mV)
Kv7.1	71.8 ± 7.9	−3.2 ± 2.1	4.6 ± 2.1*
Kv7.2	12.3 ± 6.5	−12.0 ± 0.8	−9.1 ± 2.0
Kv7.4	30.6 ± 10.3	−14.4 ± 3.6	−15.2 ± 4.3
Kv7.5	37.2 ± 5.2	−32.7 ± 5.7	−33.6 ± 6.1
Kv7.2/Kv7.3	3.6 ± 0.2	−3.9 ± 1.2	−7.5 ± 3.5

$V_{1/2}$, half activation voltage (mV); All values are the mean ± SEM.
$^{*}P < 0.05$ compared with the control, $n = 5$–10.

10 μM caused a slight rightward shift in the $V_{1/2}$ of Kv7.2 channel from −12.0 ± 0.8 mV to −9.1 ± 2.0 mV ($n = 6$). Paroxetine at 10 μM also slowed the activation kinetic of Kv7.2 channel with an increased time constant to 141.7 ± 15.8 ms from 132.6 ± 15.0 ms, while showing no significant alteration in the deactivation kinetic (from 24.9 ± 10.0 to 18.6 ± 6.9 ms) (Fig. 3C and Table 2, $n = 6$).

Reduction of single Kv7.2 channel open probability by paroxetine

We also examined the effect of paroxetine on the single-channel current of Kv7.2 channel. As shown in Fig. 4A, paroxetine at a concentration near its IC_{50} reduced Kv7.2 single-channel open probability to 0.09 ± 0.01 from 0.19 ± 0.01 ($n = 5$) without altering the channel conductance, which remained at 7.7 ± 0.7 pS from 7.7 ± 0.4 pS (Fig. 4B, $n = 5$). For comparison, perfusion with the specific Kv7 channel blocker XE991 (3 μM) similarly reduced the open probability to 0.05 ± 0.01 from 0.21 ± 0.02 (Fig. 4C, $n = 4$) without significant alteration of single-channel conductance, which remained at 8.0 ± 0.4 pS from 7.7 ± 0.8 pS (Fig. 4D, $n = 4$). These results demonstrate that paroxetine directly acts on Kv7.2/Kv7.3 and Kv7.2 channels at both macroscopic and single-channel current levels.

Selective inhibition of neuronal Kv7.2/Kv7.3 channels over other subtypes by paroxetine

We next tested the inhibitory effect of paroxetine on Kv7 subtypes from Kv7.1–Kv7.5 transiently expressed in HEK293T cells. As shown in Fig. 5 and Table 1, paroxetine at different concentrations also exhibited concentration-dependent inhibition of the channel subtypes with reduced potency for Kv7.1 (IC_{50}: 71.8 ± 7.9 μM, $n = 6$), Kv7.4 (IC_{50}: 30.6 ± 10.3 μM, $n = 5$), and Kv7.5 (IC_{50}:37.2 ± 5.2 μM, $n = 10$).

We also examined the effect of paroxetine on the voltage-dependent activation of Kv7.1, Kv7.4 and Kv7.5 channels at the concentrations near their IC_{50} values. As shown in Fig. 6A, paroxetine caused a slight rightward shift in the voltage-dependent activation of Kv7.1 with its $V_{1/2}$ shifted to a more depolarized potential at 4.6 ± 2.1 mV from −3.2 ± 2.1 mV ($n = 7$). For Kv7.4 and Kv7.5 channels, 20 μM paroxetine did not induce any significant changes in their voltage-dependent activation curves. The $V_{1/2}$ values for Kv7.4 were −15.2 ± 4.3 mV ($n = 7$) and −14.4 ± 3.6 mV under control conditions, while for Kv7.5 were −33.6 ± 6.1 mV ($n = 6$) and −32.7 ± 5.7 mV (Fig. 6B, C, and Table 1). In addition, paroxetine slowed the activation kinetic of Kv7.1 channel with an increased time constant of 98.3 ± 11.2 ms from 79.5 ± 7.7 ms ($n = 5$), and accelerated deactivation kinetic with a reduced time constant of 27.9 ± 3.6 ms from 39.9 ± 3.3 ms ($n = 5$). Paroxetine showed no significant alteration of the activation or deactivation kinetics of Kv7.4 and Kv7.5 channels (Table 2).

Inhibition of the native M-current and increase of neuronal firing by paroxetine

We further investigated the effects of paroxetine on the native M-current in hippocampal neurons. As shown in Fig. 7A, the M-current was elicited by a depolarizing potential at −20 mV followed by repolarization to −60 mV. Paroxetine at 3 and 10 μM inhibited M-current by 31.5 ± 4.6% ($n = 5$) and 52.4 ± 2.0% ($n = 16$), respectively. For comparison, XE991 at 3 μM, used as a positive control, also inhibited the M-current by 21.2 ± 2.0% ($n = 10$).

We also examined the effects of paroxetine on membrane potentials and neuronal firing in hippocampal neurons. As shown in Fig. 7B, paroxetine at 3 and 10 μM significantly depolarized the resting membrane potentials (RMP) of hippocampal neurons. The RMP shifted by 8.6 ± 1.8 mV ($n = 6$) and 14.1 ± 1.1 mV ($n = 13$), resulting in changes to −48.6 ± 2.4 mV from −57.2 ± 3.4 mV and −48.5 ± 2.0 mV from −62.2 ± 1.7 mV, respectively. Similarly, XE991 at 1 and 3 μM depolarized the RMP by 6.2 ± 2.2 mV ($n = 3$) and 9.7 ± 1.2 mV ($n = 10$), respectively (Fig. 7B). In addition, paroxetine at 3 and 10 μM significantly increased the firing activity of hippocampal neurons in response to current injection (Fig. 7C, D). These results demonstrate that paroxetine enhances hippocampal neuronal excitability through inhibition of the M-current.

Identification of key residues critical for paroxetine-mediated Kv7.2 inhibition

To identify the residues critical for paroxetine-mediated Kv7.2 inhibition, we performed the molecular docking of paroxetine to Kv7.2 (PDB: 7CR0) using the Glide model of MOE 2020. The docking predicted a potential pocket with a docking score of −7.2 (Fig. 8A). As shown in Fig. 8B, three residues, F100 in the S1 segment, D212 in the S4 segment and Y237 in the S5 (adjacent α-subunit) segment, were identified as essential for paroxetine binding. These residues facilitated interactions through π-π conjugation, H-bond, salt-bridge and π-cat interactions. Among the three residues, D212 had the lowest binding energy with paroxetine, indicating its critical role in paroxetine binding. To validate this finding, we mutated D212 to alanine and evaluated its impact on Kv7.2 inhibition by paroxetine. The D212A mutation reduced the inhibitory effect of paroxetine on both Kv7.2 D212A channel and Kv7.2 D212A/Kv7.3 heteromeric channels by approximately three-fold with increased IC_{50} values to 41.0 ± 5.6 μM ($n = 5$) and 9.2 ± 1.3 μM ($n = 8$) respectively (Fig. 8C).

Table 2. Effects of paroxetine on channel activation and deactivation kinetics of Kv7 channels.

Subfamily member	$\tau_{activation}$ (0 mV)		$\tau_{deactivation}$ (−120 mV)	
	Control	Paroxetine	Control	Paroxetine
Kv7.1	79.5 ± 7.7	98.3 ± 11.2*	39.9 ± 3.3	27.9 ± 3.6*
Kv7.2	132.6 ± 15.0	141.7 ± 15.8*	24.9 ± 10.0	18.6 ± 6.9
Kv7.4	131.5 ± 23.6	131.3 ± 22.9	12.1 ± 1.3	10.9 ± 1.6
Kv7.5	77.4 ± 5.3	79.8 ± 17.6	36.7 ± 1.7	35.4 ± 5.0
Kv7.2/Kv7.3	94.5 ± 11.0	112.8 ± 9.0*	14.4 ± 1.1	12.6 ± 0.7

τ, time constant (ms); All values are the mean ± SEM.
*$P < 0.05$ compared with the control using paired Student's *t* tests, $n = 4–7$.

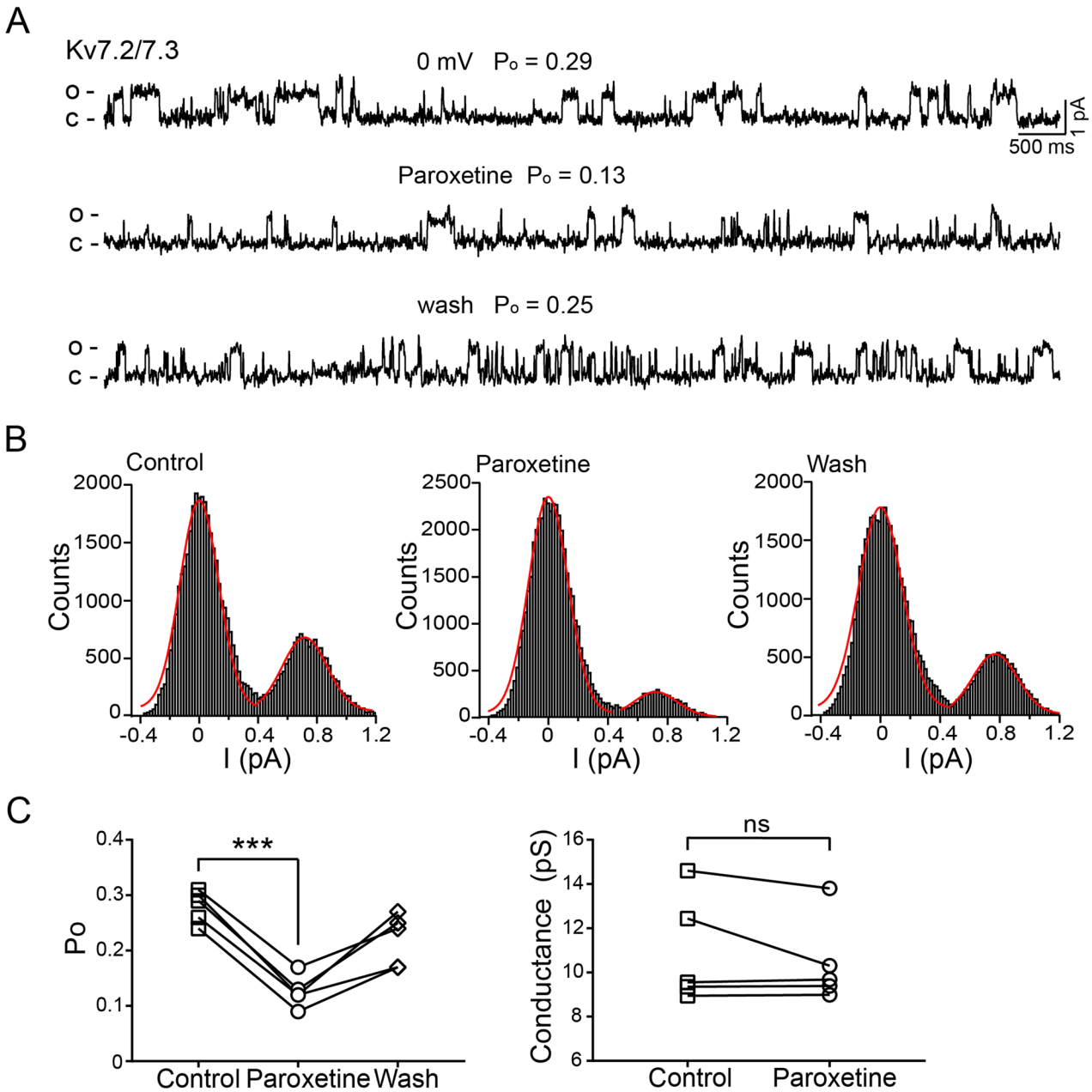

Fig. 2 Reduction of Kv7.2/Kv7.3 single channel open probability by paroxetine. A Representative single-channel (cell-attached) current traces recorded at 0 mV with or without 3 μM paroxetine. Letters O and C indicate channel open state (O) and closed state (**C**), respectively. **B** All-point amplitude histograms of single-channel currents in panel **A**. **C** Summary for effects of paroxetine on Kv7.2/Kv7.3 single-channel open probability and conductance. Paired *t*-test, ***$P < 0.001$; ns, no signification; $n = 5$.

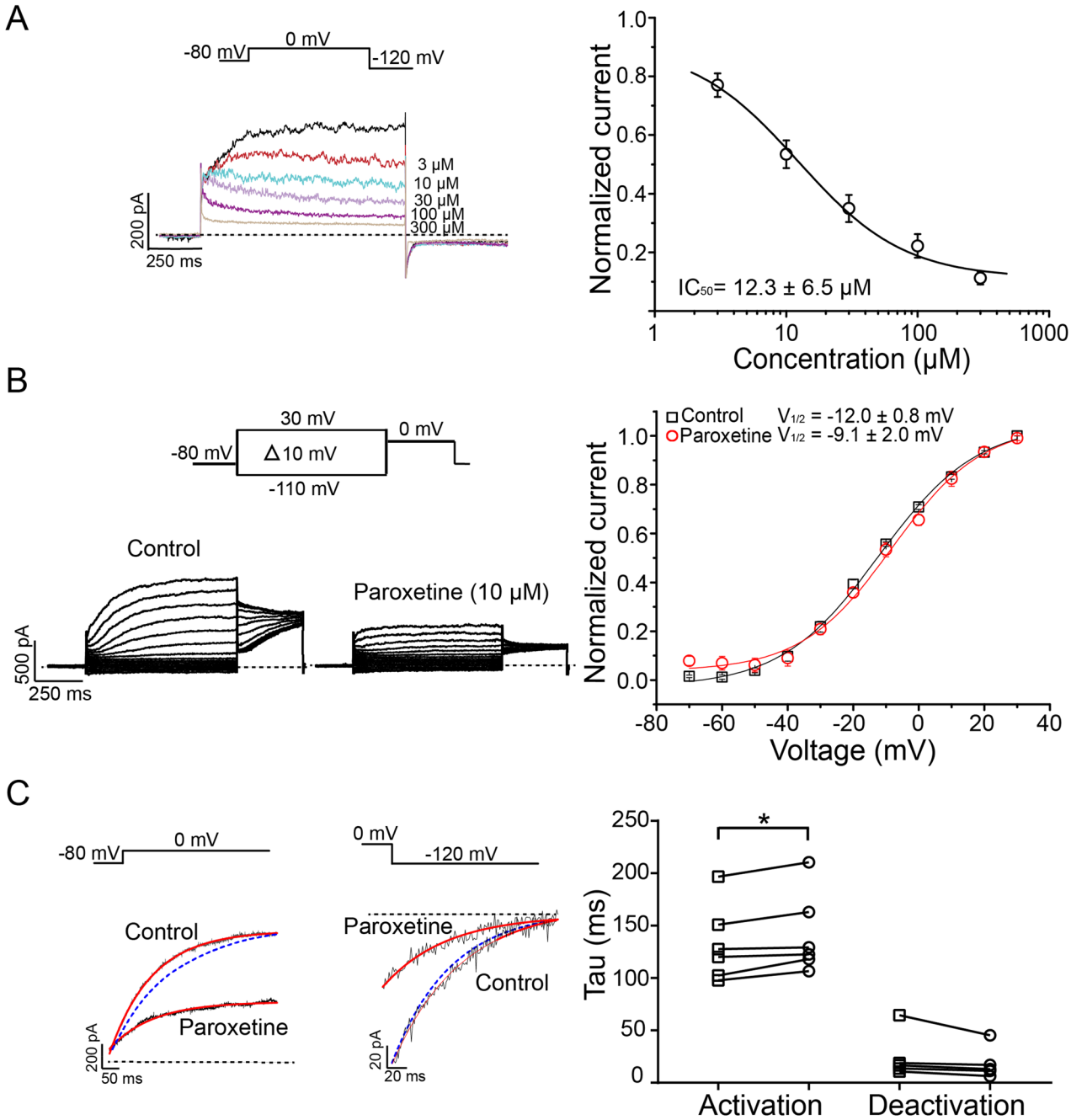

Fig. 3 Concentration-dependent inhibition of Kv7.2 currents by paroxetine. A Left panel, Representative current traces for concentration-dependent inhibition of Kv7.2 by paroxetine. The dotted line represents zero current level; Right panel, data from the left panel were fitted with Logistic function and IC_{50} of 12.3 ± 6.5 μM was obtained ($n = 9$). **B** Representative current traces of Kv7.2 channels in response to depolarizing voltage steps followed by a pulse at 0 mV in the absence (left panel) and presence (middle panel) of paroxetine; Right panel, activation curves of Kv7.2 in the absence or presence of paroxetine measured at the beginning of the 0 mV and fitted with Boltzmann function ($n = 6$). **C** Superimposed activation traces generated at 0 mV (left panel) and deactivation traces at −120 mV (middle panel) before and after paroxetine (10 μM). The current traces from paroxetine were scaled up to the same current amplitude of the control (blue dotted line); Right panel, summary of the effect of paroxetine on activation and deactivation time constants of Kv7.2 fitted with a single exponential function ($n = 6$). All data were expressed as the mean±SEM. Paired *t*-test, $^{*}P < 0.05$.

W236 in the S5 is a critical residue for retigabine-induced Kv7.2 activation [44] and ML252-induced Kv7 inhibition [45]. We next tested whether W236 as well as F240 and L299 (residues near W236) are important for paroxetine-mediated Kv7.2 inhibition. As shown in Fig. 8D, alanine mutations of these residues did not alter the sensitivity of Kv7.2 channel to 10 μM paroxetine, and the inhibition was 43.8 ± 6.8% ($n = 4$) for W236A, 46.9 ± 9.7% ($n = 3$) for F240A and 59.4 ± 10.4% ($n = 3$) for F299A, as compared to 56.6 ± 2.9% ($n = 6$) in the WT control. In addition, we investigated the effects of two other conserved Kv7 residues, F304 and F305, which are known to be important for Kv7.1 blocker-induced Kv7 inhibition [46–48]. Mutating F304 to alanine significantly reduced channel sensitivity to paroxetine by nearly three-fold, while F305A mutant had no notable effect on paroxetine-mediated inhibition of Kv7.2 (Fig. 8D). These results demonstrate that residues D212 and F304 are critical for paroxetine-induced Kv7 inhibition.

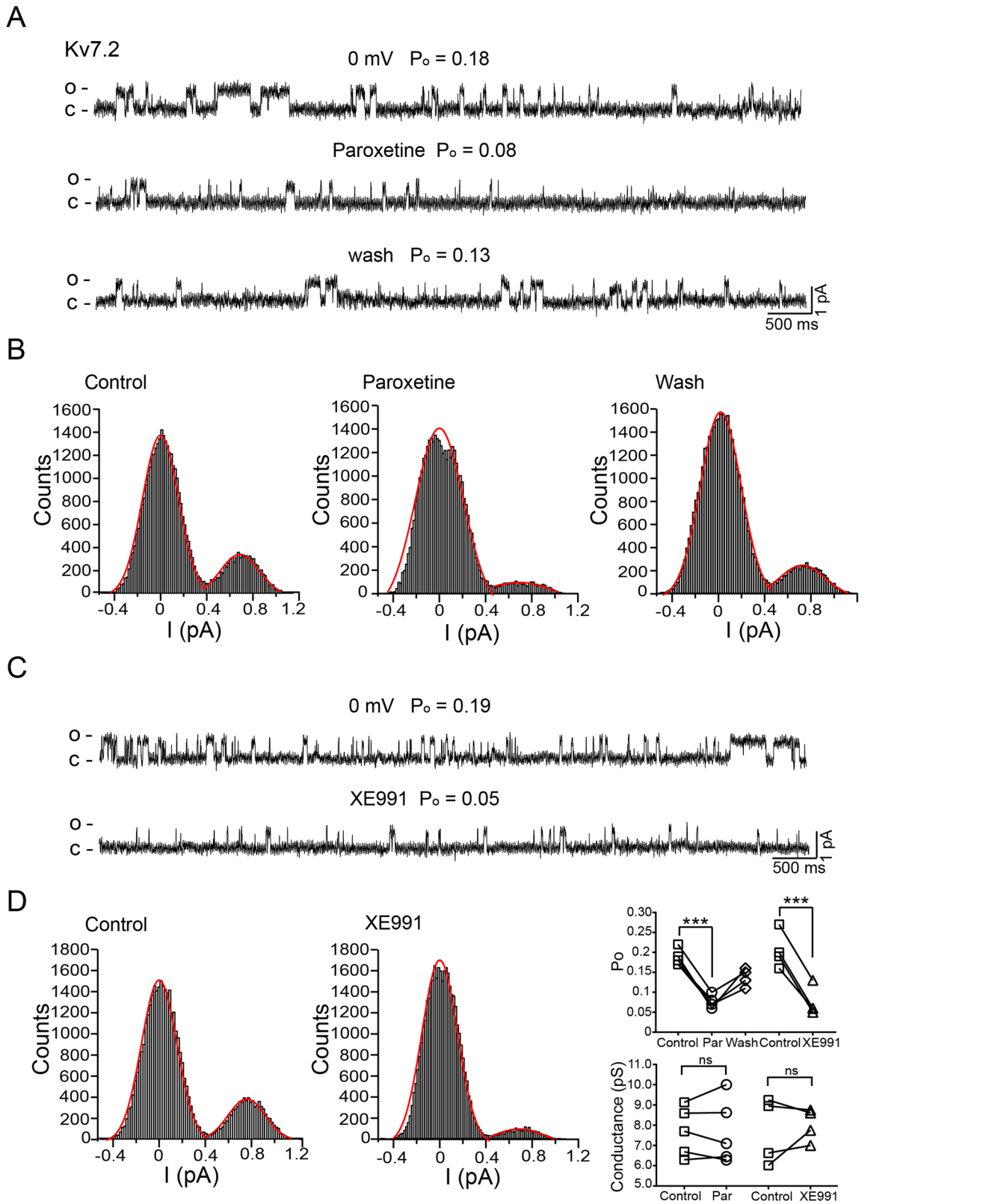

Fig. 4 Reduction of Kv7.2 single channel open probability by paroxetine. A Representative single-channel (cell-attached) current traces recorded at 0 mV with or without 10 μM paroxetine. **B** All-point amplitude histograms of single-channel currents in panel **A**. **C** Representative single-channel current traces before and after application of XE991 (3 μM). **D** Left and middle panels, all-point amplitude histograms of single-channel currents in panel **C**. Right panel, summary for effects of paroxetine and XE991 on Kv7.2 single-channel open probability and conductance. Paired *t*-test, $^{***}P < 0.001$, $n = 4–5$.

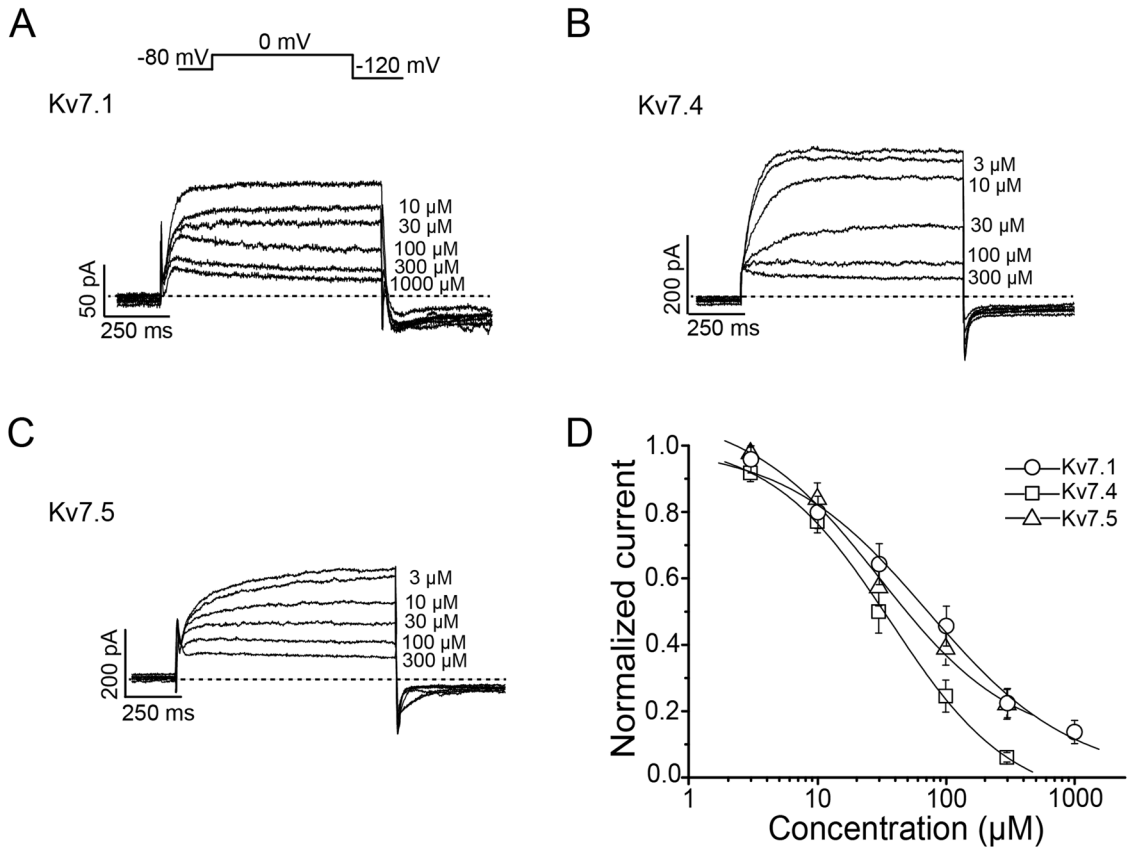

Fig. 5 Concentration-dependent inhibition of other Kv7 subtypes by paroxetine. A–**C**, Representative current traces of Kv7.1 (**A**), Kv7.4 (**B**), Kv7.5 (**C**) expressed in HEK293T cells before and after application of different concentrations of paroxetine. The dotted lines represent zero current level. **D** Concentration-dependent inhibition effect of paroxetine on Kv7 channels and fitted with Logistic function ($n = 5$–10).

However, we cannot exclude the possibility that other residues may play a significant role in paroxetine-mediated Kv7.2 inhibition.

DISCUSSION

Neuronal hypoexcitability defines the fundamental mechanisms of cognition disorders, including depression and neurodegenerative dementia. The inhibition of neuronal Kv7/KCNQ/M channels has emerged as a potential therapeutic strategy for treating cognitive deficits. This study identifies paroxetine, a selective serotonin reuptake inhibitor widely used for the treatment of depression, as an inhibitor of neuronal Kv7 channels. The following key features characterize the effects of paroxetine on Kv7 channels: 1. Paroxetine exhibits a concentration-dependent inhibition of neuronal Kv7 channels. 2. Paroxetine reduces the single-channel open probability of Kv7.2/Kv7.3 and Kv7.2 channels. 3. Paroxetine shows no significant effect on the voltage-dependent activation of neuronal Kv7 channels, except for Kv7.1. 4. Residues D212 in the S4 and F304 in the S5 segment are important for paroxetine-mediated Kv7.2 inhibition. 5. Paroxetine enhances the excitability of hippocampal neurons through inhibiting the native M-current. These findings extend the pharmacological profile of paroxetine beyond its role as a serotonin reuptake inhibitor and suggest its potential utility in addressing cognitive dysfunctions linked to neuronal hypoexcitability. The identification of key residues involved in Kv7 channel inhibition further highlights possible targets for designing more selective modulators.

Currently, only a few agents are identified as inhibitors of neuronal Kv7 channels. Among these, XE991 is a commonly used and selective Kv7 blocker, inhibiting Kv7.1-Kv7.4 channels with IC_{50} values ranging from 1–5 μM, but showing reduced sensitivity to Kv7.5 with an IC_{50} of approximately 60 μM [7, 49–52]. ML252 is another selective neuronal Kv7 inhibitor with IC_{50} values ranging from 1–6 μM [45]. Mechanistically, ML252 binds to W236 in the S5 segment, a residue conserved among Kv7.2-Kv7.5[45]. The W236 residue is also a critical binding site for Kv7 openers, including RTG, SCR2682 and ML213 [42, 44, 53]. In contrast, our data indicate that W236 is not essential for paroxetine-induced Kv7 inhibition. Instead, our molecular docking and site-directed mutagenesis identify aspartic acid residue D212 in the S4 segment as the primary interaction site for paroxetine. This residue is negatively charged and highly conserved across Kv7.1–Kv7.5. Paroxetine, as a positively charged molecule, likely forms electrostatic interactions with the negatively charged D212 residue at physiological pH conditions. This interaction may explain the broad inhibition of Kv7 channels by paroxetine.

Two additional residues, F339 and F340, are conserved among Kv7.1–Kv7.5 and have been indicated to mediate the effect of Kv7.1 blockers such as amitriptyline, chromanol 293B and benzodiazepine L-7 [46–48]. These two residues correspond to F304 and F305 in Kv7.2. Our mutational analysis reveals that the F304A mutation reduces the channel's sensitivity to paroxetine by nearly three-fold, whereas the F305A mutation does not significantly affect paroxetine-mediated inhibition of Kv7.2. This finding, together with our identification of D212 as a critical residue, underscores the importance of specific residues in the S4 and S5 segments for paroxetine-induced Kv7 inhibition. D212, being negatively charged, likely forms electrostatic interactions with the positively charged paroxetine molecule, while F304 may contribute to hydrophobic or π-stacking interactions, enhancing paroxetine's binding affinity. However,

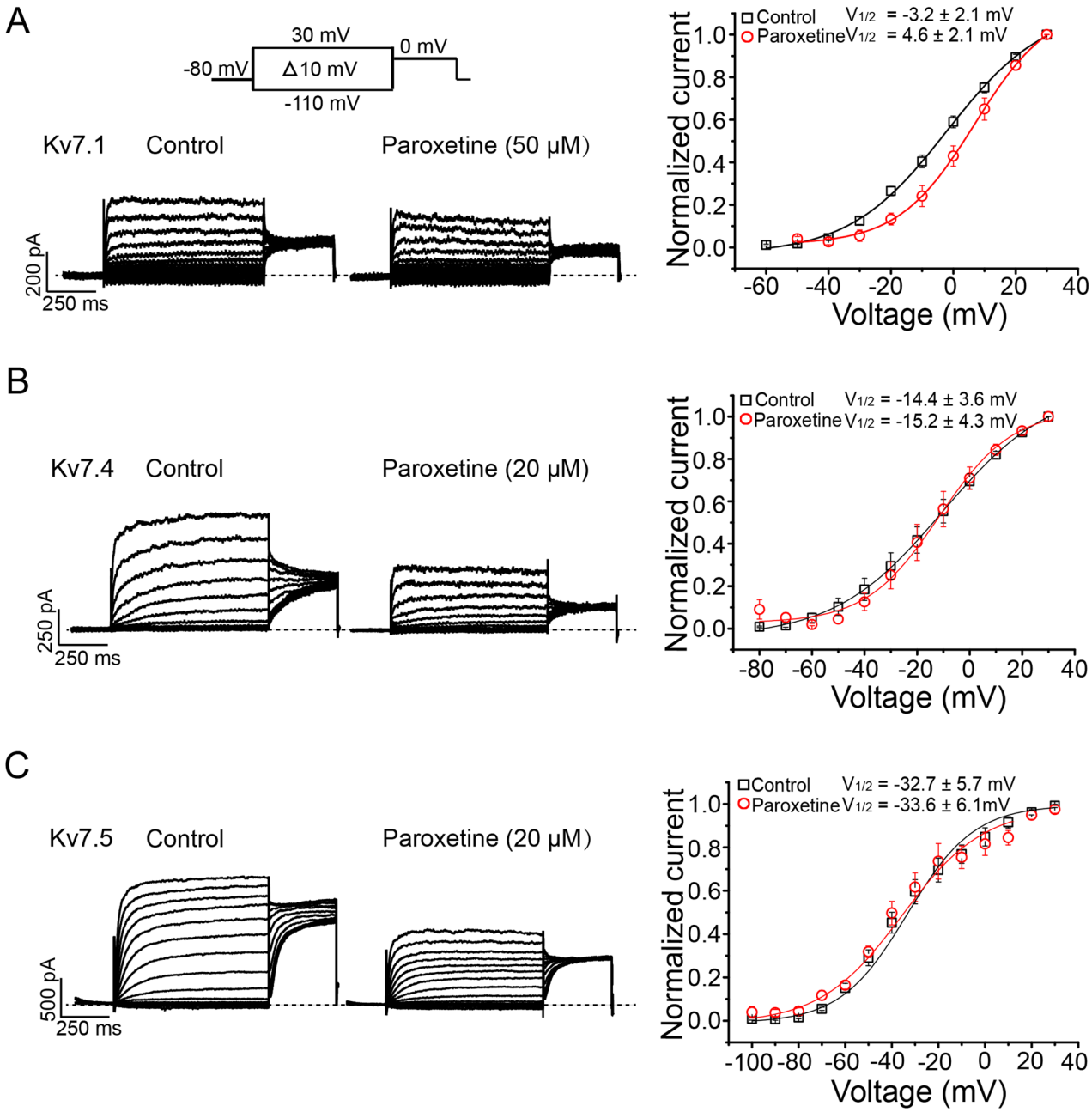

Fig. 6 The effects of paroxetine on the voltage-dependent activation of other Kv7 channels. A–C, Left and middle panels show a family of voltage-dependent currents of each Kv7 channel in the absence (left panels) and presence (middle panels) of paroxetine. The dotted lines represent zero current level; Right panels, activation curves of Kv7 channels fitted by Boltzmann function without or with paroxetine ($n = 6–7$).

we cannot rule out other residues that contribute to paroxetine-mediated Kv7 inhibition.

Paroxetine is one of the most potent and selective serotonin reuptake inhibitors. In vitro, paroxetine inhibits the serotonin transporter with a high degree of potency, exhibiting an inhibition constant (K_i) of 1.1 nM in rat hypothalamus and an IC_{50} of 30 nM in rat forebrain [54]. In vivo studies have demonstrated that oral administration of paroxetine inhibits serotonin reuptake with an ED_{50} of 1.9 mg/kg in rats [54]. In clinical settings, a typical daily dosage of 20 mg of paroxetine achieves brain concentrations ranging from approximately 2–14 μM in patients with depression [55]. This range overlaps with the IC_{50} of 3.6 μM for paroxetine inhibiting Kv7.2/Kv7.3 channels, indicating that paroxetine's inhibition of Kv7 channels could be relevant under therapeutic conditions. Paroxetine has also been reported to affect other ion channels involved in neuronal excitability. For instance, it exhibits GIRK1/2 channels with an IC_{50} of 13.8 ± 2.9 μM [39], and Kv3.1 channels with an IC_{50} of 9.4 ± 0.5 μM [40], both within the concentration range observed in the clinical applications. These findings suggest that paroxetine can enhance neuronal excitability at clinically relevant concentrations in the brain, although caution for paroxetine repurposing should be exercised for depressed patients with epilepsy.

Accumulating evidence highlights that inhibition of Kv7 channels increases neuronal excitability and plasticity, which are fundamental processes underpinning learning and memory [21]. Paroxetine improves cognitive and behavioral function in depressed patients [36], and also ameliorates the memory deficit in AD mice through functional restoration of N-methyl-D-aspartate receptor (DMDAR) subunit GluN2A [37]. NMDAR plays a pivotal

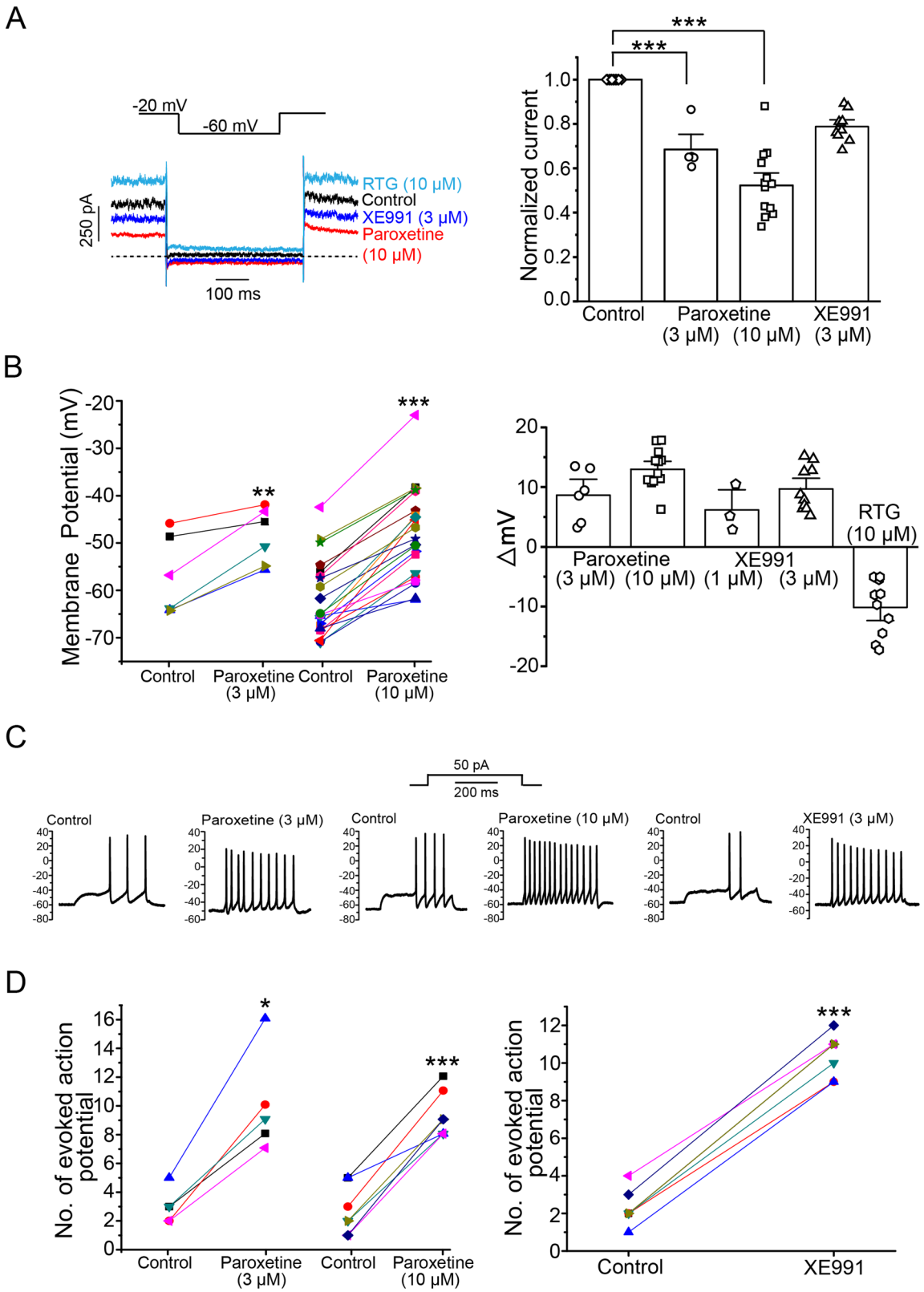

Fig. 7 Inhibition of native M-current and increase of firings in hippocampal neurons by paroxetine. A Left panel, representative M-current traces without or with 3 μM XE991, 10 μM paroxetine and 10 μM RTG recorded in hippocampal neurons. The dotted line represents the zero current level; Right panel, the inhibition effect of paroxetine (3 μM, $n = 5$; 10 μM, $n = 16$) and XE991 (3 μM, $n = 10$) on M-current measured at −20 mV. One-way ANOVA followed by Tukey test, $^{***}P < 0.001$. **B** Left panel, depolarization shift of resting membrane potentials (RMP) of hippocampal neurons by paroxetine (3 μM, $n = 6$; 10 μM, $n = 21$). Paired *t*-test, $^{**}P < 0.01$, $^{***}P < 0.001$. Right panel, statistics for changes of RMP with paroxetine (3 μM and 10 μM), XE991 (1 μM and 3 μM) and RTG (10 μM). **C** Representative action potential traces before and after application of paroxetine (3 μM and 10 μM) and XE991 (3 μM). **D** Summary for increased firings by paroxetine (3 μM, $n = 5$; 10 μM, $n = 7$; left) and 3 μM XE991 ($n = 6$; right) in hippocampal neurons. Paired *t*-test, $^{*}P < 0.05$, $^{**}P < 0.01$, $^{***}P < 0.001$.

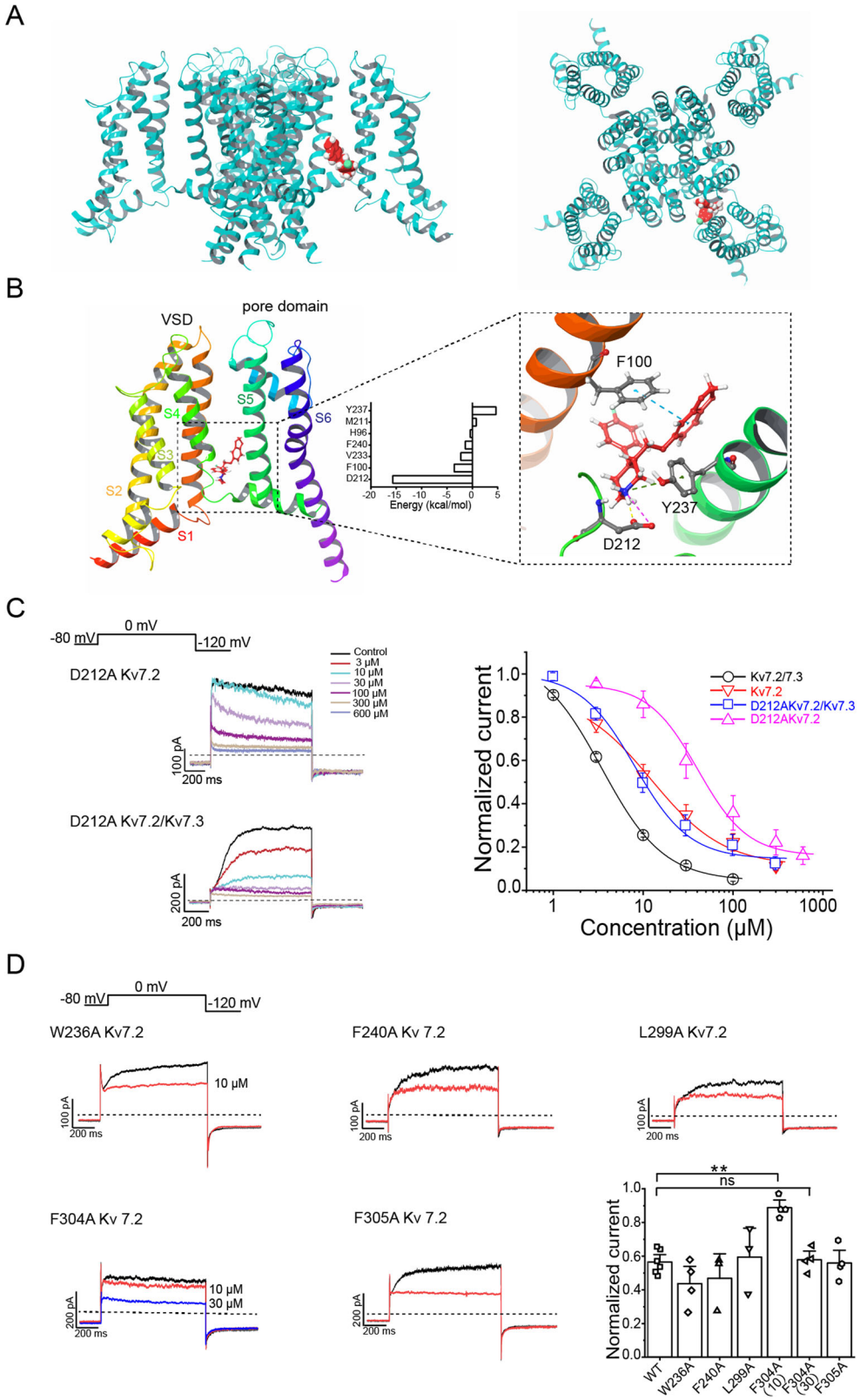

Fig. 8 The docking results of paroxetine to Kv7.2. A Side (left) and top (right) views of the predicted pocket of paroxetine binding to Kv7.2. **B** Overview of paroxetine binding to pocket and its zoom-in view of the binding pocket formed by residues F100 (S1), D212 (S4) and Y237 (S5, Adjacent α-subunit), the energy of amino acid residues in binding pocket is shown in the inset. **C** Left panels, representative current traces for concentration-dependent inhibition of D212A Kv7.2 and D212A Kv7.2/Kv7.3 by paroxetine. The dotted lines represent zero current level; Right panel, right shift of concentration-dependent inhibition of D212A Kv7.2 and D212A Kv7.2/Kv7.3 mutant channels by paroxetine in different concentrations ($n = 5–8$). **D** Representative current traces of WT Kv7.2, W236A, F240A, L299A, F304A and F305A Kv7.2 channel expressed in HEK293T cells before and after application of 10 or 30 μM paroxetine and summary of normalized inhibition effect is shown in the bottom right ($n = 3–6$). The dotted lines represent the zero current level. One-way ANOVA followed by Tukey test, $^{**}P < 0.01$, ns, no signification.

role in synaptic plasticity and learning [56, 57]. Activation of NMDAR suppresses the M-current and downregulates surface expression of Kv7 channels in hippocampal neurons through Ca^{2+}-pathways, including Ca^{2+}-PKC signaling [58] and Ca^{2+}-PI3K-PIP2 signaling [59]. These observations suggest a mechanistic interplay between NMDAR activation, Kv7 channel modulation, and enhanced neuronal excitability. Our discovery of paroxetine's novel inhibitory effect on neuronal Kv7 currents at both macroscopic and single-channel levels supports its repurposing potential as a therapeutic agent to improve memory deficits.

DATA AVAILABILITY

The authors declare that all the presented data supporting the findings of this study are contained within this paper.

REFERENCES

1. Robbins J. KCNQ potassium channels: physiology, pathophysiology, and pharmacology. Pharmacol Ther. 2001;90:1–19. https://doi.org/10.1016/s0163-7258(01)00116-4
2. Jentsch TJ. Neuronal KCNQ potassium channels: physiology and role in disease. Nat Rev Neurosci. 2000;1:21–30. https://doi.org/10.1038/35036198
3. Karlova M, Abramochkin DV, Pustovit KB, Nesterova T, Novoseletsky V, Lous-souarn G, et al. Disruption of a conservative motif in the C-terminal loop of the KCNQ1 channel causes LQT syndrome. Int J Mol Sci. 2022;23:7953. https://doi.org/10.3390/ijms23147953
4. Sanguinetti MC, Curran ME, Zou A, Shen J, Spector PS, Atkinson DL, et al. Coassembly of K(V)LQT1 and minK (IsK) proteins to form cardiac I(Ks) potassium channel. Nature. 1996;384:80–3. https://doi.org/10.1038/384080a0
5. Kharkovets T, Hardelin JP, Safieddine S, Schweizer M, El-Amraoui A, Petit C, et al. KCNQ4, a K+ channel mutated in a form of dominant deafness, is expressed in the inner ear and the central auditory pathway. Proc Natl Acad Sci USA. 2000;97:4333–8. https://doi.org/10.1073/pnas.97.8.4333
6. Peixoto Pinheiro B, Müller M, Bös M, Guezguez J, Burnet M, Tornincasa M, et al. A potassium channel agonist protects hearing function and promotes outer hair cell survival in a mouse model for age-related hearing loss. Cell Death Dis. 2022;13:595. https://doi.org/10.1038/s41419-022-04915-5
7. Wang HS, Pan Z, Shi W, Brown BS, Wymore RS, Cohen IS, et al. KCNQ2 and KCNQ3 potassium channel subunits: molecular correlates of the M-channel. Science. 1998;282:1890–3. https://doi.org/10.1126/science.282.5395.1890
8. Brown DA, Passmore GM. Neural KCNQ (Kv7) channels. Br J Pharmacol. 2009;156:1185–95. https://doi.org/10.1111/j.1476-5381.2009.00111.x
9. Brown DA, Adams PR. Muscarinic suppression of a novel voltage-sensitive K+ current in a vertebrate neurone. Nature. 1980;283:673–6. https://doi.org/10.1038/283673a0
10. Yoon JY, Ho WK. Involvement of Ca(2+) in signaling mechanisms mediating muscarinic inhibition of M currents in sympathetic neurons. Cell Mol Neurobiol. 2023;43:2257–71. https://doi.org/10.1007/s10571-022-01303-7
11. Marrion NV. Control of M-current. Annu Rev Physiol. 1997;59:483–504. https://doi.org/10.1146/annurev.physiol.59.1.483
12. Estacion M, Liu S, Cheng X, Dib-Hajj S, Waxman SG. Kv7-specific activators hyperpolarize resting membrane potential and modulate human iPSC-derived sensory neuron excitability. Front Pharmacol. 2023;14:1138556. https://doi.org/10.3389/fphar.2023.1138556
13. Wulff H, Castle NA, Pardo LA. Voltage-gated potassium channels as therapeutic targets. Nat Rev Drug Discov. 2009;8:982–1001. https://doi.org/10.1038/nrd2983
14. Liu Y, Bian X, Wang K. Pharmacology of potassium channels. Handb. Exp. Pharmacol. 2021;458:231–51.
15. Yue C, Yaari Y. KCNQ/M channels control spike afterdepolarization and burst generation in hippocampal neurons. J Neurosci. 2004;24:4614–24. https://doi.org/10.1523/jneurosci.0765-04.2004
16. Brown JT, Randall AD. Activity-dependent depression of the spike after-depolarization generates long-lasting intrinsic plasticity in hippocampal CA3 pyramidal neurons. J Physiol. 2009;587:1265–81. https://doi.org/10.1113/jphysiol.2008.167007
17. Baculis BC, Zhang J, Chung HJ. The role of K(v)7 channels in neural plasticity and behavior. Front Physiol. 2020;11:568667. https://doi.org/10.3389/fphys.2020.568667
18. Suzuki E, Okada T. Stratum oriens stimulation-evoked modulation of hippocampal long-term potentiation involves the activation of muscarinic acetylcholine receptors and the inhibition of Kv7/M potassium ion channels. Eur J Neurosci. 2012;36:1984–92. https://doi.org/10.1111/j.1460-9568.2012.08127.x
19. Petrovic MM, Nowacki J, Olivo V, Tsaneva-Atanasova K, Randall AD, Mellor JR. Inhibition of post-synaptic Kv7/KCNQ/M channels facilitates long-term potentiation in the hippocampus. PLoS One. 2012;7:e30402. https://doi.org/10.1371/journal.pone.0030402
20. Wang J, Yu W, Gao Q, Ju C, Wang K. Prefrontal inhibition of neuronal K(v) 7 channels enhances prepulse inhibition of acoustic startle reflex and resistance to hypofrontality. Br J Pharmacol. 2020;177:4720–33. https://doi.org/10.1111/bph.15236
21. Nicoll RA. A brief history of long-term potentiation. Neuron. 2017;93:281–90. https://doi.org/10.1016/j.neuron.2016.12.015
22. Brioni JD, Curzon P, Buckley MJ, Arneric SP, Decker MW. Linopirdine (DuP996) facilitates the retention of avoidance training and improves performance of septal-lesioned rats in the water maze. Pharmacol Biochem Behav. 1993;44:37–43. https://doi.org/10.1016/0091-3057(93)90278-2
23. Fontán-Lozano A, Suárez-Pereira I, Delgado-García JM, Carrión AM. The M-current inhibitor XE991 decreases the stimulation threshold for long-term synaptic plasticity in healthy mice and in models of cognitive disease. Hippocampus. 2011;21:22–32. https://doi.org/10.1002/hipo.20717
24. Kosenko A, Moftakhar S, Wood MA, Hoshi N. In vivo attenuation of M-Current suppression impairs consolidation of object recognition memory. J Neurosci. 2020;40:5847–56. https://doi.org/10.1523/jneurosci.0348-20.2020
25. Millan MJ, Agid Y, Brüne M, Bullmore ET, Carter CS, Clayton NS, et al. Cognitive dysfunction in psychiatric disorders: characteristics, causes and the quest for improved therapy. Nat Rev Drug Discov. 2012;11:141–68. https://doi.org/10.1038/nrd3628
26. Rock PL, Roiser JP, Riedel WJ, Blackwell AD. Cognitive impairment in depression: a systematic review and meta-analysis. Psychol Med. 2014;44:2029–40. https://doi.org/10.1017/s0033291713002535
27. McDermott LM, Ebmeier KP. A meta-analysis of depression severity and cognitive function. J Affect Disord. 2009;119:1–8. https://doi.org/10.1016/j.jad.2009.04.022
28. Matcham F, Simblett SK, Leightley D, Dalby M, Siddi S, Haro JM, et al. The association between persistent cognitive difficulties and depression and functional outcomes in people with major depressive disorder. Psychol Med. 2023;53:6334–44. https://doi.org/10.1017/s0033291722003671
29. Bourin M, Chue P, Guillon Y. Paroxetine: a review. CNS Drug Rev. 2001;7:25–47. https://doi.org/10.1111/j.1527-3458.2001.tb00189.x
30. Kowalska M, Nowaczyk J, Fijałkowski Ł, Nowaczyk A. Paroxetine-overview of the molecular mechanisms of action. Int J Mol Sci. 2021;22:1662. https://doi.org/10.3390/ijms22041662
31. Jannini TB, Lorenzo GD, Bianciardi E, Niolu C, Toscano M, Ciocca G, et al. Off-label uses of selective serotonin reuptake inhibitors (SSRIs). Curr Neuropharmacol. 2022;20:693–712. https://doi.org/10.2174/1570159x19666210517150418
32. Balci M, Atan A, Senel C, Guzel O, Aslan Y, Lokman U, et al. Comparison of the treatment efficacies of paroxetine, fluoxetine and dapoxetine in low socio-economic status patients with lifelong premature ejaculation. Cent European J Urol. 2019;72:185–90. https://doi.org/10.5173/ceju.2019.1855
33. Safarinejad MR. Comparison of dapoxetine versus paroxetine in patients with premature ejaculation: a double-blind, placebo-controlled, fixed-dose, randomized study. Clin Neuropharmacol. 2006;29:243–52. https://doi.org/10.1097/01.Wnf.0000228210.12194.46
34. Slaton RM, Champion MN, Palmore KB. A review of paroxetine for the treatment of vasomotor symptoms. J Pharm Pract. 2015;28:266–74. https://doi.org/10.1177/0897190014544785
35. David PS, Smith TL, Nordhues HC, Kling JM. A clinical review on paroxetine and emerging therapies for the treatment of vasomotor symptoms. Int J Womens Health. 2022;14:353–61. https://doi.org/10.2147/ijwh.S282396
36. Cassano GB, Puca F, Scapicchio PL, Trabucchi M. Paroxetine and fluoxetine effects on mood and cognitive functions in depressed nondemented elderly patients. J Clin Psychiatry. 2002;63:396–402.
37. Ai PH, Chen S, Liu XD, Zhu XN, Pan YB, Feng DF, et al. Paroxetine ameliorates prodromal emotional dysfunction and late-onset memory deficit in Alzheimer's disease mice. Transl Neurodegener. 2020;9:18. https://doi.org/10.1186/s40035-020-00194-2
38. Nelson RL, Guo Z, Halagappa VM, Pearson M, Gray AJ, Matsuoka Y, et al. Prophylactic treatment with paroxetine ameliorates behavioral deficits and retards the development of amyloid and tau pathologies in 3xTgAD mice. Exp Neurol. 2007;205:166–76. https://doi.org/10.1016/j.expneurol.2007.01.037
39. Kobayashi T, Washiyama K, Ikeda K. Inhibition of G Protein-activated inwardly rectifying K+ channels by the antidepressant paroxetine. J Pharmacol Sci. 2006;102:278–87. https://doi.org/10.1254/jphs.FP0060708
40. Lee HM, Chai OH, Hahn SJ, Choi BH. Antidepressant drug paroxetine blocks the open pore of Kv3.1 potassium channel. Korean J Physiol Pharmacol. 2018;22:71–80. https://doi.org/10.4196/kjpp.2018.22.1.71

41. Brewer GJ, Torricelli JR, Evege EK, Price PJ. Optimized survival of hippocampal neurons in B27-supplemented Neurobasal, a new serum-free medium combination. J Neurosci Res. 1993;35:567–76. https://doi.org/10.1002/jnr.490350513
42. Zhang F, Liu Y, Tang F, Liang B, Chen H, Zhang H, et al. Electrophysiological and pharmacological characterization of a novel and potent neuronal Kv7 channel opener SCR2682 for antiepilepsy. FASEB J. 2019;33:9154–66. https://doi.org/10.1096/fj.201802848RR
43. Li Y, Gamper N, Shapiro MS. Single-channel analysis of KCNQ K+channels reveals the mechanism of augmentation by a cysteine-modifying reagent. J Neurosci. 2004;24:5079–90. https://doi.org/10.1523/jneurosci.0882-04.2004
44. Schenzer A, Friedrich T, Pusch M, Saftig P, Jentsch TJ, Grötzinger J, et al. Molecular determinants of KCNQ (Kv7) K+ channel sensitivity to the anticonvulsant retigabine. J Neurosci. 2005;25:5051–60. https://doi.org/10.1523/jneurosci.0128-05.2005
45. Kanyo R, Lamothe SM, Urrutia A, Goodchild SJ, Allison WT, Dean R, et al. Site and mechanism of ML252 inhibition of Kv7 voltage-gated potassium channels. Function. 2023;4:zqad021 https://doi.org/10.1093/function/zqad021
46. Villatoro-Gómez K, Pacheco-Rojas DO, Moreno-Galindo EG, Navarro-Polanco RA, Tristani-Firouzi M, Gazgalis D, et al. Molecular determinants of Kv7.1/KCNE1 channel inhibition by amitriptyline. Biochem Pharmacol. 2018;152:264–71. https://doi.org/10.1016/j.bcp.2018.03.016
47. Lerche C, Bruhova I, Lerche H, Steinmeyer K, Wei AD, Strutz-Seebohm N, et al. Chromanol 293B binding in KCNQ1 (Kv7.1) channels involves electrostatic interactions with a potassium ion in the selectivity filter. Mol Pharmacol. 2007;71:1503–11. https://doi.org/10.1124/mol.106.031682
48. Seebohm G, Chen J, Strutz N, Culberson C, Lerche C, Sanguinetti MC. Molecular determinants of KCNQ1 channel block by a benzodiazepine. Mol Pharmacol. 2003;64:70–77. https://doi.org/10.1124/mol.64.1.70
49. Søgaard R, Ljungstrøm T, Pedersen KA, Olesen SP, Jensen BS. KCNQ4 channels expressed in mammalian cells: functional characteristics and pharmacology. Am J Physiol Cell Physiol. 2001;280:C859–866. https://doi.org/10.1152/ajpcell.2001.280.4.C859
50. Wang HS, Brown BS, McKinnon D, Cohen IS. Molecular basis for differential sensitivity of KCNQ and I(Ks) channels to the cognitive enhancer XE991. Mol Pharmacol. 2000;57:1218–23.
51. Schroeder BC, Hechenberger M, Weinreich F, Kubisch C, Jentsch TJ. KCNQ5, a novel potassium channel broadly expressed in brain, mediates M-type currents. J Biol Chem. 2000;275:24089–95. https://doi.org/10.1074/jbc.M003245200
52. Jensen HS, Callø K, Jespersen T, Jensen BS, Olesen SP. The KCNQ5 potassium channel from mouse: a broadly expressed M-current like potassium channel modulated by zinc, pH, and volume changes. Brain Res Mol Brain Res. 2005;139:52–62. https://doi.org/10.1016/j.molbrainres.2005.05.007
53. Yu H, Wu M, Hopkins C, Engers J, Townsend S, Lindsley C et al. Probe reports from the NIH molecular libraries program. Bethesda (MD): National Center for Biotechnology Information (US); 2010.
54. Johnson AM. An overview of the animal pharmacology of paroxetine. Acta Psychiatr Scand Suppl. 1989;350:14–20. https://doi.org/10.1111/j.1600-0447.1989.tb07161.x
55. Henry ME, Moore CM, Kaufman MJ, Michelson D, Schmidt ME, Stoddard E, et al. Brain kinetics of paroxetine and fluoxetine on the third day of placebo substitution: a fluorine MRS study. Am J Psychiatry. 2000;157:1506–8. https://doi.org/10.1176/appi.ajp.157.9.1506
56. Paoletti P, Bellone C, Zhou Q. NMDA receptor subunit diversity: impact on receptor properties, synaptic plasticity and disease. Nat Rev Neurosci. 2013;14:383–400. https://doi.org/10.1038/nrn3504
57. Traynelis SF, Wollmuth LP, McBain CJ, Menniti FS, Vance KM, Ogden KK, et al. Glutamate receptor ion channels: structure, regulation, and function. Pharmacol Rev. 2010;62:405–96. https://doi.org/10.1124/pr.109.002451
58. Li C, Lu Q, Huang P, Fu T, Li C, Guo L, et al. Activity-dependent downregulation of M-Type (Kv7) K^+ channels surface expression requires the activation of iGluRs/Ca^{2+}/PKC signaling pathway in hippocampal neuron. Neuropharmacology. 2015;95:154–67. https://doi.org/10.1016/j.neuropharm.2015.03.004
59. Zhang H, Sheng ZF, Wang J, Zheng P, Kang X, Chang HM, et al. Signaling pathways involved in NMDA-induced suppression of M-channels in corticotropin-releasing hormone neurons in central amygdala. J Neurochem. 2022;161:478–91. https://doi.org/10.1111/jnc.15647

ACKNOWLEDGEMENTS
We are grateful to Dr. X Tang for his help in the molecular modeling.

AUTHOR CONTRIBUTIONS
HS, QL performed the experiments and analyzed the data. FH, YL, and KW designed the experiments and supervised the study. HS drafted and YL, and KW revised and finalized the manuscript. All authors have agreed to all manuscript contents.

FUNDING
This work was supported by National Natural Science Foundation of China (82104149 for YL and 81973299, 32471204 for KW), National Natural Science Foundation of Shandong Province (ZR2020QH100 for YL).

COMPETING INTERESTS
The authors declare no competing interests.

ETHICS APPROVAL
All methods were performed in accordance with the relevant guidelines and regulations approved by the Ethics Committee of Qingdao University Medical College (Approval No. QDU-AEC-2021105). This study did not involve human participants and animals.

INFORMED CONSENT
Informed consent was obtained from all participants.

ADDITIONAL INFORMATION
Correspondence and requests for materials should be addressed to Yani Liu or KeWei Wang.